Chapter 9. Deterministic Chaos

This chapter gives a very brief review of chaotic phenomena in deterministic maps and dynamic systems with and without dissipation, and an even shorter discussion of the possible role of chaos in fluid turbulence.

9.1. Chaos in maps

The possibility of quasi-random dynamics of deterministic systems with a few degrees of freedom (nowadays called *deterministic chaos* – or just "chaos") had been noticed before the 20th century,[1] but became broadly recognized only after the publication of a 1963 paper by theoretical meteorologist Edward Lorenz. In that work, he examined numerical solutions of the following system of three nonlinear, ordinary differential equations,

Lorenz system

$$\begin{aligned} \dot{q}_1 &= a_1(q_2 - q_1), \\ \dot{q}_2 &= a_2 q_1 - q_2 - q_1 q_3, \\ \dot{q}_3 &= q_1 q_2 - a_3 q_3, \end{aligned} \tag{9.1}$$

as a rudimentary model of heat transfer through a horizontal layer of fluid separating two solid plates. (Experiment shows that if the bottom plate is kept hotter than the top one, the fluid may exhibit turbulent convection.) He has found that within a certain range of the constants $a_{1,2,3}$, the solution to Eq. (1) follows complex, unpredictable, non-repeating trajectories in the 3D q-space. Moreover, the functions $q_j(t)$ (where j = 1, 2,3) are so sensitive to initial conditions $q_j(0)$ that at sufficiently large times t, solutions corresponding to slightly different initial conditions become completely different.

Very soon it was realized that such behavior is typical for even simpler mathematical objects called *maps*, so I will start my discussion of chaos from these objects. A 1D map is essentially a rule for finding the next number q_{n+1} of a discrete sequence numbered by the integer index n, in the simplest cases using only its last known value q_n. The most famous example is the so-called *logistic map*:[2]

Logistic map

$$q_{n+1} = f(q_n) \equiv r q_n (1 - q_n). \tag{9.2}$$

The basic properties of this map may be understood using its (hopefully, self-explanatory) graphical representation shown in Fig. 1.[3] One can readily see that at $r < 1$ (Fig. 1a) the logistic map sequence rapidly converges to the trivial fixed point $q^{(0)} = 0$ because each next value of q is less than the previous one. However, if r is increased above 1 (as in the example shown in Fig. 1b), the fixed point

[1] It may be traced back at least to an 1892 paper by the same Jules Henri Poincaré who was already reverently mentioned in Chapter 5. Citing it: "*...it may happen that small differences in the initial conditions produce very great ones in the final phenomena*. […] *Prediction becomes impossible*."

[2] Its chaotic properties were first discussed in 1976 by Robert May, though the map itself is one of the simple ecological models repeatedly discussed much earlier and may be traced back at least to the 1838 work by Pierre François Verhulst.

[3] Since the maximum value of the function $f(q)$, achieved at q = ½, equals r/4, the mapping may be limited to segment x = [0, 1], if the parameter r is between 0 and 4. Since all interesting properties of the map, including chaos, may be found within these limits, I will discuss only this range of r.

$q^{(0)}$ becomes unstable. Indeed, at $q_n << 1$, the map yields $q_{n+1} \approx rq_n$, so at $r > 1$, the values q_n grow with each iteration. Instead of the unstable point $q^{(0)} = 0$, in the range $1 < r < r_1$, where $r_1 \equiv 3$, the map has a stable fixed point $q^{(1)}$ that may be found by plugging this value into both parts of Eq. (2):

$$q^{(1)} = f\left(q^{(1)}\right) \equiv rq^{(1)}(1-q^{(1)}), \tag{9.3}$$

giving $q^{(1)} = 1 - 1/r$ – see the leftmost branch of the plot shown in Fig. 2.

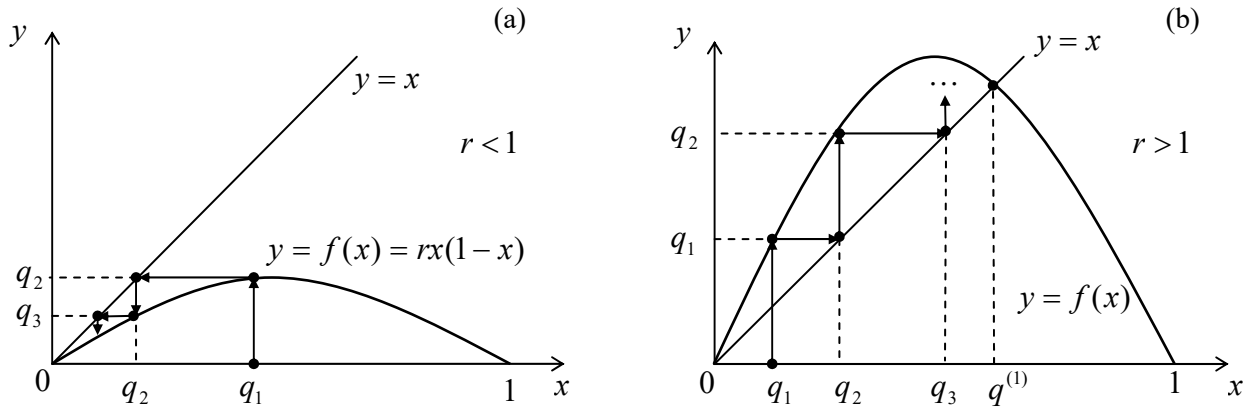

Fig. 9.1. Graphical analysis of the logistic map for: (a) $r < 1$ and (b) $r > 1$.

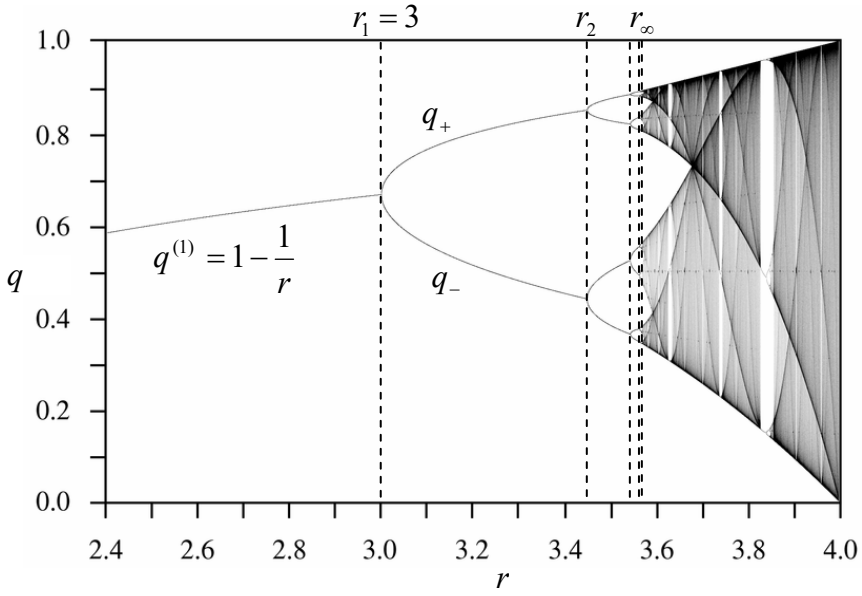

Fig. 9.2. The fixed points and chaotic regions of the logistic map. Adapted, under the CCO 1.0 Universal Public Domain Dedication, from the original by Jordan Pierce, available at http://en.wikipedia.org/wiki/Logistic_map. (A very nice live simulation of the map is also available on this website.)

However, at $r > r_1 = 3$, the fixed point $q^{(1)}$ also becomes unstable. To prove that, let us take $q_n \equiv q^{(1)} + \tilde{q}_n$, assume that the deviation $\tilde{q}_n$ from the fixed point $q^{(1)}$ is small, and linearize the map (2) in $\tilde{q}_n$ – just as we repeatedly did for differential equations earlier in this course. The result is

$$\tilde{q}_{n+1} = \left.\frac{df}{dq}\right|_{q=q^{(1)}} \tilde{q}_n = r(1-2q^{(1)})\tilde{q}_n \equiv (2-r)\tilde{q}_n . \tag{9.4}$$

It shows that at $0 < 2 - r < 1$, i.e. at $1 < r < 2$, the deviations $\tilde{q}_n$ decrease monotonically. At $-1 < 2 - r < 0$, i.e. in the range $2 < r < 3$, the deviations' sign alternates, but their magnitude still decreases – as in a stable focus, see Sec. 5.6. However, at $-1 < 2 - r$, i.e. $r > r_1 \equiv 3$, the deviations grow by magnitude, while still changing their sign, at each step. Since Eq. (2) has no other fixed points, this means that at $n \to \infty$, the values q_n do not converge to one point; rather, within the range $r_1 < r < r_2$, they approach a *limit cycle* of alternation of two points, q_+ and q_-, that satisfy the following system of algebraic equations:

$$q_+ = f(q_-), \qquad q_- = f(q_+). \tag{9.5}$$

These points are also plotted in Fig. 2, as functions of the parameter r. What has happened at the point $r_1 = 3$ is called the *period-doubling bifurcation*.

The story repeats at $r = r_2 \equiv 1 + \sqrt{6} \approx 3.45$, where the system goes from the 2-point limit cycle to a 4-point cycle, then at $r = r_3 \approx 3.54$, where the limit cycle begins to consist of 8 alternating points, etc. Most remarkably, the period-doubling bifurcation points r_n, at that the number of points in the limit cycle doubles from 2^{n-1} points to 2^n points, become closer and closer to each other. Numerical simulations show that at $n \to \infty$, these points obey the following asymptotic behavior:

Feigenbaum bifurcation sequence

$$r_n \to r_\infty - \frac{C}{\delta^n}, \quad \text{where } r_\infty = 3.5699..., \quad \delta = 4.6692... \tag{9.6}$$

The parameter δ is called the *Feigenbaum constant*; for other maps, and some dynamic systems (see the next section), period-doubling sequences follow a similar law, but with different values of δ.

More important for us, however, is what happens at $r > r_\infty$. Numerous numerical experiments, repeated with increasing precision,[4] have confirmed that here the system is disordered, with no reproducible limit cycle, though (as Fig. 2 shows) at $r \approx r_\infty$, all sequential values q_n are still confined to a few narrow regions.[5] However, as parameter r is increased well beyond r_∞, these regions broaden and merge. This is the so-called *deep chaos*, with no apparent order at all.[6]

The most important feature of the chaos (in this and any other system) is the *exponential divergence of trajectories*. For a 1D map, this means that even if the initial conditions q_1 in two map implementations differ by a very small amount Δq_1, the difference Δq_n between the corresponding sequences q_n is growing, on average, exponentially with n. Such exponents may be used to characterize chaos. Indeed, an evident generalization of the linearized Eq. (4) to an arbitrary point q_n is

$$\Delta q_{n+1} = e_n \Delta q_n, \qquad e_n \equiv \left. \frac{df}{dq} \right|_{q=q_n}. \tag{9.7}$$

[4] The reader should remember that just like the usual ("nature") experiments, numerical experiments also have limited accuracy, due to unavoidable rounding errors.

[5] The geometry of these regions is essentially *fractal*, i.e. has a dimensionality intermediate between 0 (which any final set of geometric points would have) and 1 (pertinent to a 1D continuum). An extensive discussion of fractal geometries and their relation to deterministic chaos may be found, for example, in the book by B. Mandelbrot, *The Fractal Geometry of Nature*, W. H. Freeman, 1983.

[6] This does not mean that chaos depth is always a monotonic function of r. As Fig. 2 shows, within certain intervals of this parameter, the chaotic behavior suddenly disappears, being replaced, typically, with a few-point limit cycle, just to resume on the other side of the interval. Sometimes (but not always!) the "route to chaos" on the borders of these intervals follows the same Feigenbaum sequence of period-doubling bifurcations.

Let us assume that Δq_1 is so small that N first values q_n are relatively close to each other. Then using Eq. (7) iteratively for these steps, we get

$$\Delta q_N = \Delta q_1 \prod_{n=1}^{N} e_n, \qquad \text{so that} \quad \ln\left|\frac{\Delta q_N}{\Delta q_1}\right| = \sum_{n=1}^{N} \ln|e_n|. \tag{9.8}$$

Numerical experiments show that in most chaotic regimes, at $N \to \infty$ such a sum fluctuates about an average, which grows as λN, with the parameter

$$\lambda \equiv \lim_{\Delta q_1 \to 0} \lim_{N \to \infty} \frac{1}{N} \sum_{n=1}^{N} \ln|e_n|, \tag{9.9}$$

Lyapunov exponent

called the *Lyapunov exponent*,[7] being independent of the initial conditions. The bottom panel in Fig. 3 shows λ as a function of the parameter r for the logistic map (2). (Its top panel shows the same pattern as Fig. 2, which is reproduced here just for the sake of comparison.)

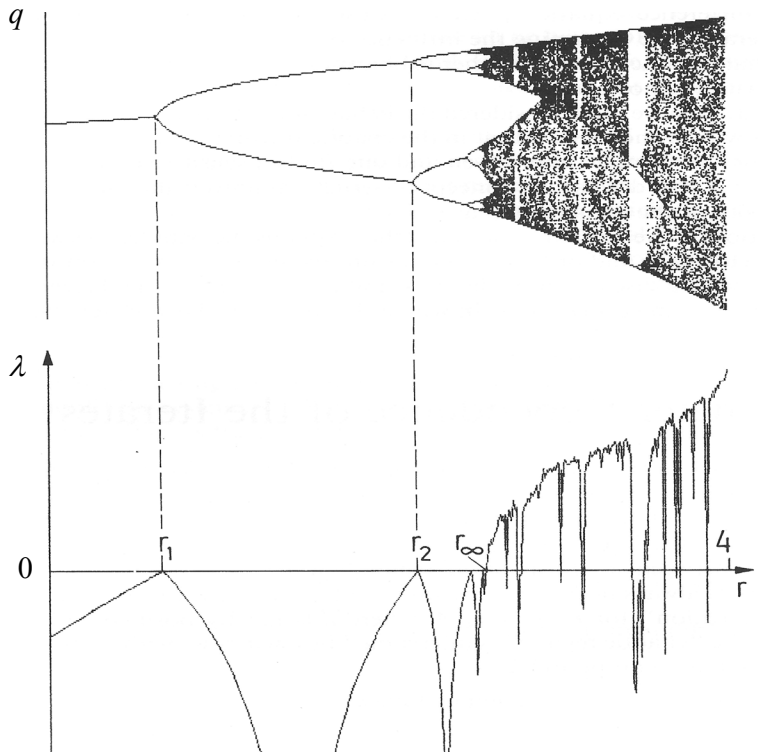

Fig. 9.3. The Lyapunov exponent for the logistic map. Adapted, with permission, from the monograph by Schuster and Just (cited below). © Wiley-VCH Verlag GmbH & Co. KGaA.

Note that at $r < r_\infty$, λ is negative, indicating the sequence's stability, besides the points r_1, r_2, … where λ would become positive if the limit cycle changes (bifurcations) had not brought it back into the negative territory. However, at $r > r_\infty$, λ becomes positive, returning to negative values only in limited intervals of stable limit cycles. It is evident that in numerical experiments (which dominate the studies of deterministic chaos) the Lyapunov exponent may be used as a good measure of the chaos' depth.[8]

[7] After Alexandr Mikhailovich Lyapunov (1857-1918), famous for his studies of the stability of dynamic systems.

[8] N-dimensional maps that relate N-dimensional vectors rather than scalars, may be characterized by N Lyapunov exponents rather than one. For chaotic behavior, it is sufficient for just one of them to become positive. For such systems, another measure of chaos, the *Kolmogorov entropy,* may be more relevant. This measure and its relation with the Lyapunov exponents are discussed, for example, in SM Sec. 2.2.

Despite the abundance of results published for particular maps,[9] and several interesting observations (like the already discussed existence of the Feigenbaum bifurcation sequences), to the best of my knowledge, nobody can yet predict the patterns like those shown in Fig. 2 and 3 by just studying the mapping rule itself, i.e. without carrying out actual numerical experiments. Unfortunately, the understanding of deterministic chaos in other systems is not much better.

9.2. Chaos in dynamic systems

Proceeding to the discussion of chaos in dynamic systems, it is more natural, with our background, to illustrate this discussion not with the Lorenz equations, but with the system of equations describing a dissipative pendulum driven by a sinusoidal external force, which was repeatedly discussed in Chapter 5. Introducing two new variables, the normalized momentum $p \equiv (dq/dt)/\omega_0$, and the external force's full phase $\psi \equiv \omega t$, we may rewrite Eq. (5.42), describing the pendulum, in a form similar to Eq. (1), i.e. as a system of three first-order ordinary differential equations:

$$\begin{aligned} \dot{q} &= \omega_0 p, \\ \dot{p} &= -\omega_0 \sin q - 2\delta p + (f_0/\omega_0)\cos\psi, \\ \dot{\psi} &= \omega. \end{aligned} \tag{9.10}$$

Figure 4 shows several results of a numerical solution of Eq. (10).[10] In all cases, parameters δ, ω_0, and f_0 are fixed, while the external frequency ω is gradually changed. For the case shown on the top two panels, the system still tends to a stable periodic solution, with very low contents of higher harmonics. If the external force frequency is reduced by a just few percent, the 3rd subharmonic may be excited. (This effect has already been discussed in Sec. 5.8 – see, e.g., Fig. 5.15.) The next row shows that just a small further reduction of the frequency ω leads to a new tripling of the period, i.e. the generation of a complex waveform with the 9th subharmonic. Finally (see the bottom panels of Fig. 4), even a minor further change of ω leads to oscillations without any visible period, e.g., to the chaos.

In order to trace this transition, a direct inspection of the oscillation waveforms $q(t)$ is not very convenient, and trajectories on the phase plane $[q, p]$ also become messy if plotted for many periods of the external frequency. In situations like this, the Poincaré (or "stroboscopic") plane, already discussed in Sec. 5.6, is much more useful. As a reminder, this is essentially just the phase plane $[q, p]$, but with the points highlighted only once a period, e.g., at $\psi = 2\pi n$, with $n = 1, 2, \ldots$ On this plane, periodic oscillations of frequency ω are represented just as one fixed point – see, e.g. the top panel in the right column of Fig. 4. The 3rd subharmonic generation, shown on the next panel, means the oscillation period's tripling and is represented as the splitting of the fixed point into three. It is evident that this transition is similar to the period-doubling bifurcation in the logistic map, besides the fact (already discussed in Sec. 5.8) that in systems with an antisymmetric nonlinearity, such as the pendulum (10), the 3rd subharmonic is easier to excite. From this point, the 9th harmonic generation (shown on the 3rd panel of Fig. 4), i.e. one more splitting of the points on the Poincaré plane, may be understood as one more step on the Feigenbaum-like route to chaos – see the bottom panel of that figure.

---

[9] See, e.g., Chapters 2-4 in H. Schuster and W. Just, *Deterministic Chaos*, 4th ed., Wiley-VCH, 2005, or Chapters 8-9 in J. Thompson and H. Stewart, *Nonlinear Dynamics and Chaos*, 2nd ed., Wiley, 2002.

[10] In the actual simulation, a small term εq, with $\varepsilon << 1$, has been added to the left-hand side of this equation. This term slightly tames the trend of the solution to spread along the q-axis, and makes the presentation of results easier, without affecting the system's dynamics too much.

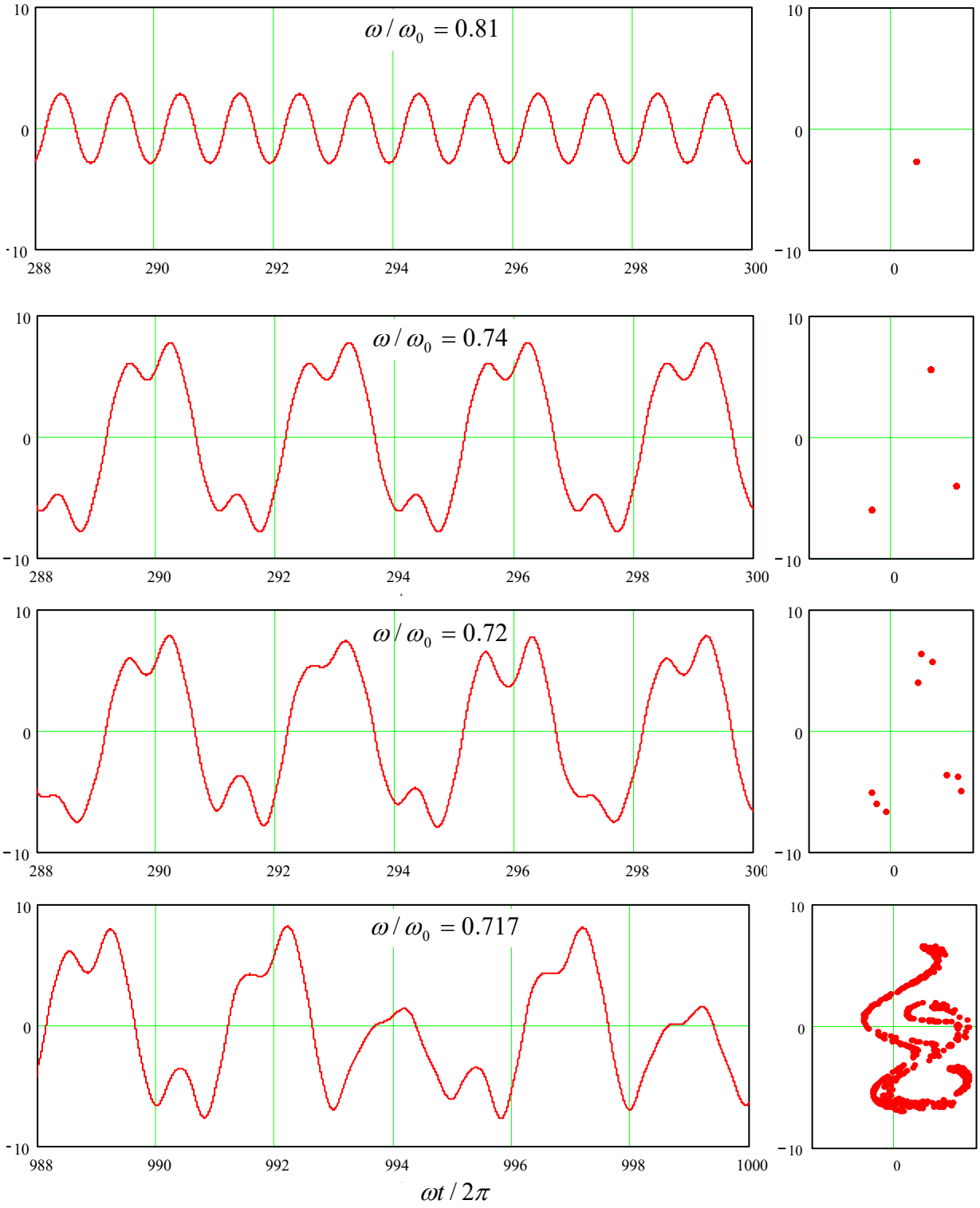

Fig. 9.4. Oscillations in a pendulum with weak damping, $\delta/\omega_0 = 0.1$, driven by a sinusoidal external force with a fixed effective amplitude $f_0/\omega_0^2 = 1$, and several close values of the frequency ω (listed on the panels). Left panel column: the oscillation waveforms $q(t)$ recorded after certain initial transient intervals. Right column: representations of the same processes on the Poincaré plane of the variables $[q, p]$, with the q-axis turned vertically, for the convenience of comparison with the left panels.

So, the transition to chaos in dynamic systems may be at least qualitatively similar to that in 1D maps, with a law similar to Eq. (6) for the critical values of some parameter of the system (in Fig. 4, frequency ω), though with a system-specific value of the coefficient δ. Moreover, we may consider the first two differential equations of the system (10) as a 2D map that relates the vector $\{q_{n+1}, p_{n+1}\}$ of the coordinate and momentum, measured at $\psi = 2\pi(n + 1)$, with the previous value $\{q_n, p_n\}$ of that vector, reached at $\psi = 2\pi n$.

Unfortunately, this similarity also implies that the deterministic chaos in dynamic systems is at least as complex, and is as little understood, as in maps. For example, Fig. 5 shows (a part of) the phase diagram of the externally-driven pendulum, with the red bar marking the route to chaos traced in Fig. 4, and shading/hatching styles marking different oscillation regimes. One can see that the pattern is at least as complex as that shown in Figs. 2 and 3, and, besides a few features,[11] is equally unpredictable from the form of the equation.

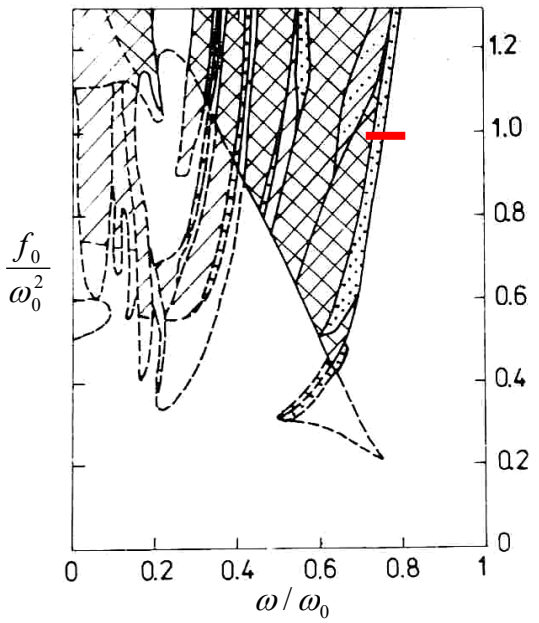

Fig. 9.5. The phase diagram of an externally driven pendulum with weak damping ($\delta/\omega_0 = 0.1$). The regions of oscillations with the basic period are not shaded; the notation for other regions is as follows. Doted: subharmonic generation; cross-hatched: chaos; hatched: either chaos or the basic period (depending on the initial conditions); hatch-dotted: either the basic period or subharmonics. Solid lines show the boundaries of single-regime regions, while dashed lines are the boundaries of the regions where several types of motion are possible. (Figure courtesy by V. Kornev.)

Are there any valuable general results concerning the deterministic chaos in dynamic systems? The most important (though an almost evident) result is that this phenomenon is impossible in any system described by one or two first-order differential equations with time-independent right-hand sides. Indeed, let us start with a single equation

$$\dot{q} = f(q), \tag{9.11}$$

where $f(q)$ is any single-valued function. This equation may be directly integrated to give

$$t = \int^{q} \frac{dq'}{f(q')} + \text{const}, \tag{9.12}$$

showing that the relation between q and t is unique and hence does not leave any place for chaos.

[11] In some cases, it is possible to predict a parameter region where chaos *cannot* happen, due to the lack of any instability-amplification mechanism. Unfortunately, typically the analytically predicted boundaries of such a region form a rather loose envelope of the actual (numerically simulated) chaotic regions.

Next, let us explore a system of two such equations:

$$\begin{aligned} \dot{q}_1 &= f_1(q_1, q_2), \\ \dot{q}_2 &= f_2(q_1, q_2). \end{aligned} \tag{9.13}$$

Consider its phase plane shown schematically in Fig. 6. In a "usual" system, the trajectories approach either some fixed point (Fig. 6a) describing static equilibrium, or a limit cycle (Fig. 6b) describing periodic oscillations. (Both notions are united by the term *attractor* because they "attract" trajectories launched from various initial conditions.) On the other hand, phase plane trajectories of a chaotic system of equations that describe physical variables (which cannot be infinite), should be confined to a limited phase plane area, and simultaneously cannot start repeating each other. (This topology is frequently called the *strange attractor*.) For that, the 2D trajectories need to cross – see, e.g., point A in Fig. 6c.

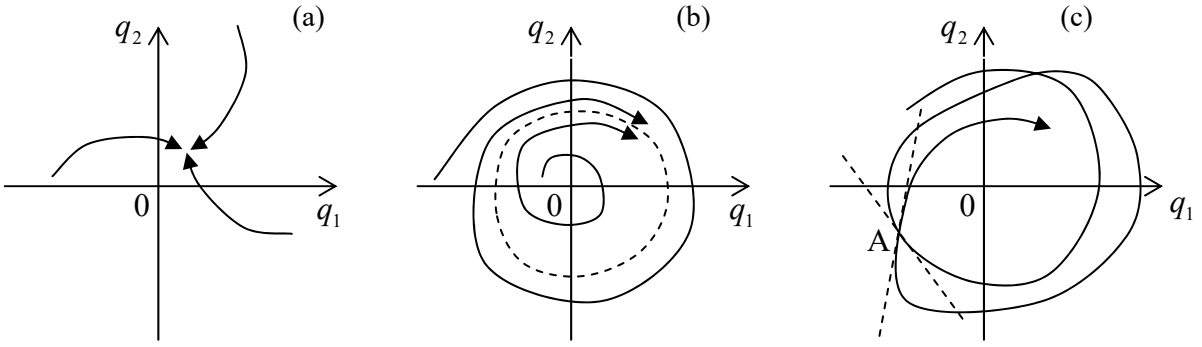

Fig. 9.6. Attractors in dynamical systems: (a) a fixed point, (b) a limit cycle, and (c) a strange attractor.

However, in the case described by Eqs. (13), such a crossing is clearly impossible, because according to these equations, the tangent of a phase plane trajectory is a unique function of the coordinates $\{q_1, q_2\}$:

$$\frac{dq_1}{dq_2} = \frac{f_1(q_1, q_2)}{f_2(q_1, q_2)}. \tag{9.14}$$

Thus, in this case, the deterministic chaos is impossible.[12] It becomes, however, readily possible if the right-hand sides of a system similar to Eq. (13) depend either on other variables of the system or time. For example, if we consider the first two differential equations of the system (10), in the case $f_0 = 0$ they have the structure of the system (13), and hence the chaos is impossible – even at $\delta < 0$ when (as we know from Sec. 5.4) the system allows self-excitation of oscillations, leading to a limit-cycle attractor. However, if $f_0 \neq 0$, this argument does not work any longer, and (as we have already seen) the system may have a strange attractor – which is, for dynamic systems, a synonym for the deterministic chaos.

Thus, chaos is only possible in autonomous dynamic systems described by three or more differential equations of the first order.[13]

[12] A mathematically strict formulation of this statement is called the *Poincaré-Bendixon theorem*, which was proved by Ivar Bendixon in 1901.

[13] Since a typical dynamic system with one degree of freedom is described by two such equations, the number of first-order equations describing a dynamic system is sometimes called the number of its *half-degrees of freedom.* This notion is very useful and popular in statistical mechanics – see, e.g., SM Sec. 2.2 and on.

9.3. Chaos in Hamiltonian systems

The last conclusion is of course valid for Hamiltonian systems, which are just a particular type of dynamic systems. However, one may wonder whether these systems, which feature at least one first integral of motion, H = const, and hence are more "ordered" than the systems discussed above, can exhibit chaos at all. The answer is *yes* because such systems still can have mechanisms for the exponential growth of a small initial perturbation.

As the simplest way to show it, let us consider the so-called *mathematical billiard*, i.e. system with a ballistic particle (a "ball") moving freely by inertia on a horizontal plane surface ("table") limited by rigid walls. In this idealized model of the usual game of billiards, the ball's velocity $\mathbf{v}$ is conserved when it moves on the table, and when it runs into a wall, the ball is elastically reflected from it as from a mirror,[14] with the reversal of the sign of the normal velocity v_n, and the conservation of the tangential velocity v_τ, and hence without any loss of its kinetic (and hence the full) energy

$$E = H = T = \frac{m}{2}v^2 = \frac{m}{2}\left(v_n^2 + v_\tau^2\right). \tag{9.15}$$

This model, while being a legitimate 2D dynamic system,[15] allows geometric analyses for several simple table shapes. The simplest of them is a rectangular billiard of area $a \times b$ (Fig. 7), whose analysis may be readily carried out just by the replacement of each *ball* reflection event with the mirror reflection of the *table* in that wall – see the dashed lines on panel (a).

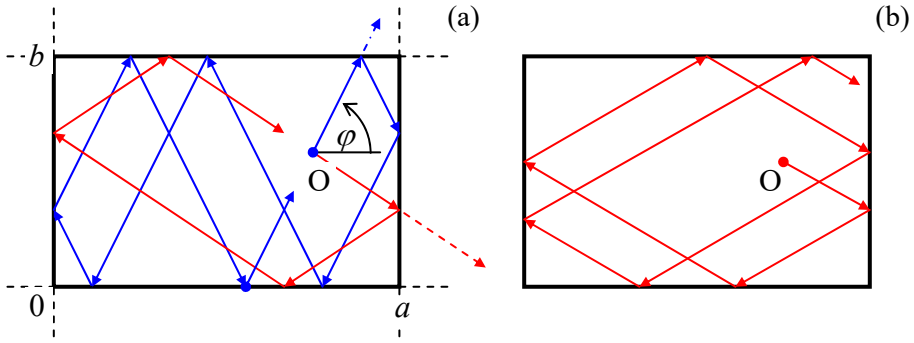

Fig. 9.7. Ball motion on a rectangular billiard at (a) a commensurate, and (b) an incommensurate launch angle.

Such analysis (left for the reader's pleasure :-) shows that if the tangent of the ball launching angle φ is commensurate with the side length ratio:

$$\tan\varphi = \pm\frac{m}{n}\frac{b}{a}, \tag{9.16}$$

where n and m are non-negative integers without common integer multipliers, the ball returns exactly to the launch point O, after bouncing m times from each wall of length a, and n times from each wall of length b. (Red lines in Fig. 7a show an example of such a trajectory for $n = m = 1$, while blue lines, for $m = 3$, $n = 1$.) The larger is the sum $(m + n)$, the more complex is such a closed "orbit".

[14] A more scientific-sounding name for such a reflection is *specular* – from the Latin word "speculum" meaning a metallic mirror.

[15] Indeed, it is fully described by the following Lagrangian function: $L = mv^2/2 - U(\boldsymbol{\rho})$, with $U(\boldsymbol{\rho}) = 0$ for the 2D radius vectors $\boldsymbol{\rho}$ belonging to the table area, and $U(\boldsymbol{\rho}) = +\infty$ outside the area.

Finally, if $(n + m) \to \infty$, i.e. $\tan\varphi$ and b/a are incommensurate (meaning that their ratio is an irrational number), the trajectory covers all of the table area, and the ball never returns exactly to the launch point. Still, this is not genuine chaos. Indeed, a small shift of the launch point O shifts all the trajectory fragments by the same displacement. Moreover, at any time t, each of Cartesian components $v_j(t)$ of the ball's velocity (with coordinate axes parallel to the table sides) may take only two values, $\pm v_j(0)$, and hence may vary only as much as the initial velocity is being changed.

In 1963, i.e. well before E. Lorenz's work, Yakov Sinai showed that the situation changes completely if an additional wall, in the shape of a circle, is inserted into the rectangular billiard (Fig. 8). For most initial conditions, the ball's trajectory eventually runs into the circle (see the red line on panel (a) as an example), and the further trajectory becomes essentially chaotic. Indeed, let us consider the ball's reflection from a circle-shaped wall – Fig. 8b. Due to the conservation of the tangential velocity, and the sign change of the normal velocity component, the reflection obeys a simple law: $\theta_r = \theta_i$. Figure 8b shows that as the result, the magnitude of a small difference $\delta\varphi$ between the angles of two close trajectories (as measured in the lab system), doubles at each reflection from the curved wall. This means that the small deviation grows along the ball trajectory as

$$\left|\delta\varphi(N)\right| \sim \left|\delta\varphi(0)\right| \times 2^N \equiv \left|\delta\varphi(0)\right| e^{N \ln 2}, \tag{9.17}$$

where N is the number of reflections from the convex wall.[16] As we already know, such exponential divergence of trajectories, with a positive Lyapunov exponent, is the main feature of deterministic chaos.[17]

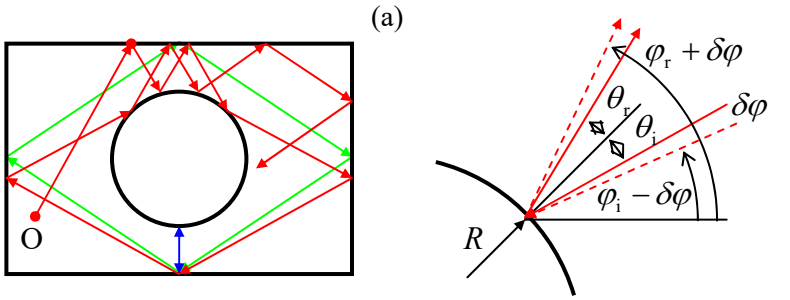

Fig. 9.8. (a) Motion on a Sinai billiard table, and (b) the mechanism of the exponential divergence of close trajectories.

The most important new feature of the dynamic chaos in Hamiltonian systems is its dependence on initial conditions. (In the systems discussed in the previous two sections, that lack the integrals of motion, the initial conditions are rapidly "forgotten", and the chaos is usually characterized after an initial transient period – see, e.g., Fig. 4.) Indeed, even a Sinai billiard allows periodic motion, along closed orbits, under certain initial conditions – see the blue and green lines in Fig. 8a as examples. Thus

[16] Superficially, Eq. (17) is also valid for a plane wall, but as was discussed above, a billiard with such walls features a full correlation between sequential reflections, so angle φ always returns to its initial value. In a Sinai billiard, such correlation disappears. Concave walls may also make a billiard chaotic; a famous example is the *stadium billiard*, suggested by Leonid Bunimovich in 1974, with two straight, parallel walls connecting two semi-circular, concave walls. Another example, which allows a straightforward analysis (first carried out by Martin Gutzwiller in the 1980s), is the so-called *Hadamard billiard*: an infinite (or rectangular) table with a non-horizontal surface of negative curvature.

[17] Curved-wall billiards are also a convenient platform for studies of quantum properties of classically chaotic systems (for their conceptual discussion, see QM Sec. 3.5), in particular, the features called "quantum scars" – see, e.g., the spectacular numerical simulation results by E. Heller, *Phys. Rev. Lett.* **53**, 1515 (1984).

the chaos "depth" in such systems may be characterized by the "fraction"[18] of the phase space of initial parameters (for a 2D billiard, of the 3D space of the initial values of x, y, and φ) resulting in chaotic trajectories.

This conclusion is also valid for Hamiltonian systems that are met in physics much more frequently than exotic billiards, for example, coupled nonlinear oscillators without damping. Perhaps the earliest and the most popular example is the so-called *Hénon-Heiles* system,[19] which may be described by the following Lagrangian function:

$$L = \frac{m_1}{2}\left(\dot{q}_1^2 - \omega_1^2 q_1^2\right) + \frac{m_2}{2}\left(\dot{q}_2^2 - \omega_2^2 q_2^2\right) - \varepsilon\left(q_1^2 - \frac{1}{3}q_2^2\right)q_2 . \tag{9.18}$$

Hénon-Heiles system

It is straightforward to use this function to derive the corresponding Lagrange equations of motion,

$$\begin{aligned} m_1\left(\ddot{q}_1 + \omega_1^2 q_1\right) &= -2\varepsilon q_1 q_2 , \\ m_2\left(\ddot{q}_2 + \omega_2^2 q_2\right) &= -\varepsilon\left(q_1^2 - q_2^2\right), \end{aligned} \tag{9.19}$$

and find their first integral of motion (physically, the energy conservation law):

$$H = E = \frac{m_1}{2}\left(\dot{q}_1^2 + \omega_1^2 q_1^2\right) + \frac{m_2}{2}\left(\dot{q}_2^2 + \omega_2^2 q_2^2\right) + \varepsilon\left(q_1^2 - \frac{1}{3}q_2^2\right)q_2 = \text{const} . \tag{9.20}$$

In the context of our discussions in Chapters 5 and 6, Eqs. (19) may be readily interpreted as those describing two oscillators, with small-oscillation frequencies ω_1 and ω_2, coupled only by the quadratic terms on the right-hand sides of the equations. This means that as the oscillation amplitudes $A_{1,2}$, and hence the total energy E of the system, are close to zero, the oscillator subsystems are virtually independent, each performing sinusoidal oscillations at its own frequency. This observation suggests a convenient way to depict the system's motion.[20] Let us consider a Poincaré plane for one of the oscillators (say, with coordinate q_2), similar to that discussed in Sec. 2 above, with the only difference is that (because of the absence of an explicit function of time in the system's equations), the trajectory on the phase plane $[q_2, \dot{q}_2]$ is highlighted at the moments when $q_1 = 0$.

Let us start from the limit $A_{1,2} \to 0$ when the oscillations of q_2 are virtually sinusoidal. As we already know (see Fig. 5.9 and its discussion), if the representation point highlighting was perfectly synchronous with frequency ω_2 of the oscillations, there would be only one point on the Poincaré plane – see, e.g. the right top panel of Fig. 4. However, at the q_1 – initiated highlighting, there is no such synchronism, so each period, a different point of the elliptical (at the proper scaling of the velocity,

[18] Actually, quantitative characterization of the fraction is not trivial, because it may have *fractal dimensionality*. Unfortunately, due to lack of time I have to refer the reader interested in this issue to special literature, e.g., the monograph by B. Mandelbrot (cited above) and references therein.

[19] It was first studied in 1964 by M. Hénon and C. Heiles as a simple model of star rotation about a galactic center. Most studies of this equation have been carried out for the following particular case: $m_2 = 2m_1$, $m_1\omega_1^2 = m_2\omega_2^2$. In this case, by introducing new variables $x \equiv \varepsilon q_1$, $y \equiv \varepsilon q_2$, and $\tau \equiv \omega_1 t$, it is possible to rewrite Eqs. (19) in a parameter-free form. All the results shown in Fig. 9 below are for this case.

[20] Generally, the system has a trajectory in 4D space, e.g., that of coordinates $q_{1,2}$ and their time derivatives, although the first integral of motion (20) means that for each fixed energy E, the motion is limited to a 3D subspace. Still, this is one dimension too many for a convenient representation of the motion.

circular) trajectory is highlighted, so the resulting points, for certain initial conditions, reside on a circle of radius A_2. If we now vary the initial conditions, i.e. redistribute the initial energy between the oscillators, but keep the total energy E constant, on the Poincaré plane we get a set of ellipses.

Now, if the initial energy is increased, the nonlinear interaction of the oscillations starts to deform these ellipses, causing also their crossings – see, e.g., the top left panel of Fig. 9. Still, below a certain threshold value of E, all Poincaré points belonging to a certain initial condition sit on a single closed contour. Moreover, these contours may be calculated approximately, but with pretty good accuracy, using a straightforward generalization of the method discussed in Sec. 5.2.[21]

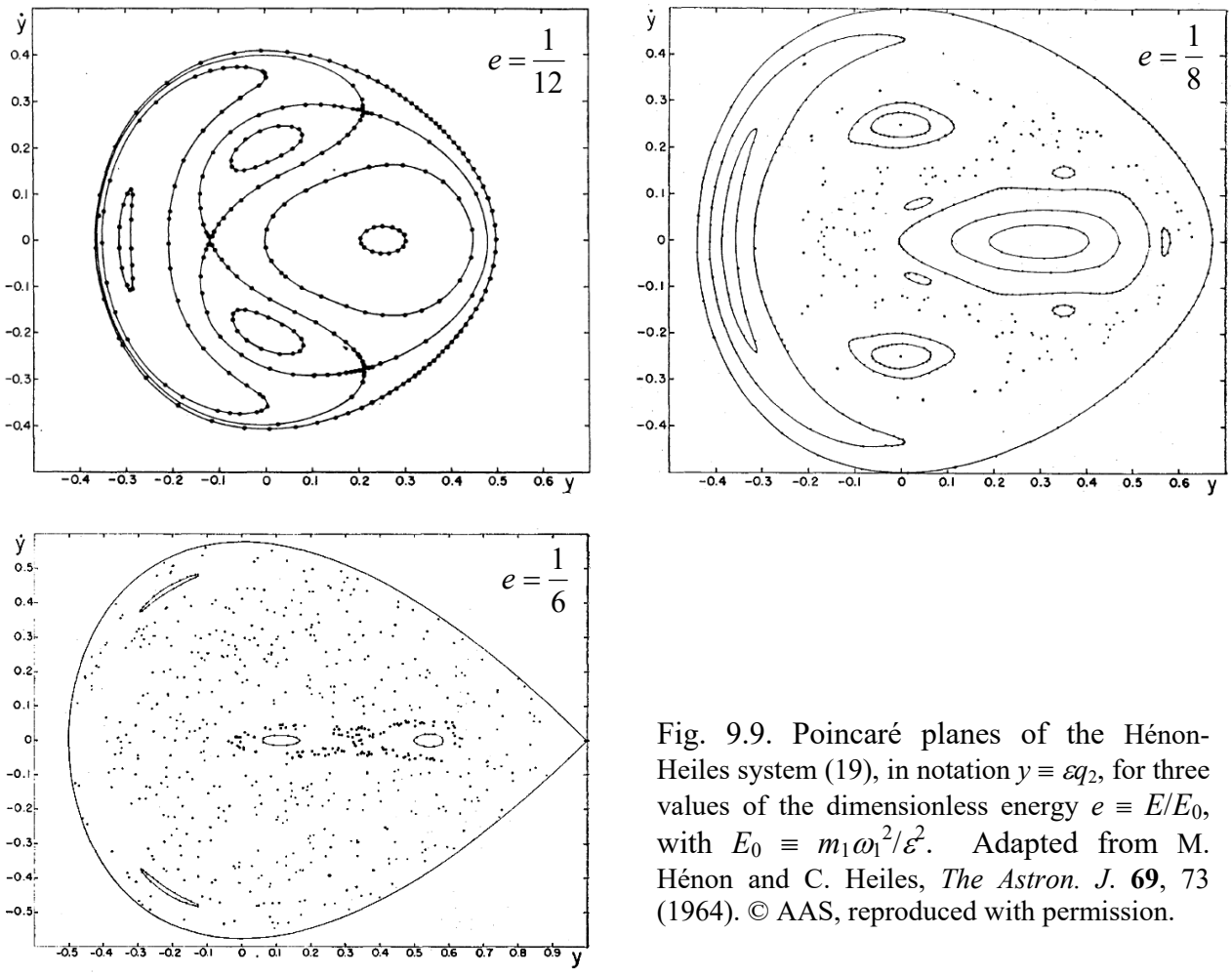

Fig. 9.9. Poincaré planes of the Hénon-Heiles system (19), in notation $y \equiv \varepsilon q_2$, for three values of the dimensionless energy $e \equiv E/E_0$, with $E_0 \equiv m_1\omega_1^2/\varepsilon^2$. Adapted from M. Hénon and C. Heiles, *The Astron. J.* **69**, 73 (1964). © AAS, reproduced with permission.

However, starting from some value of energy, certain initial conditions lead to sequences of points scattered over parts of the Poincaré plane, with a nonzero area – see the top right panel of Fig. 9. This means that the corresponding oscillations $q_2(t)$ do not repeat from one (quasi-) period to the next one – cf. Fig. 4 for the dissipative, forced pendulum. This is chaos.[22] Still, some other initial conditions

[21] See, e.g., M. Berry, in: S. Jorna (ed.), *Topics in Nonlinear Dynamics*, AIP Conf. Proc. No. 46, AIP, 1978, pp. 16-120.

[22] This fact complies with the necessary condition of chaos, discussed at the end of Sec. 2, because Eqs. (19) may be rewritten as a system of *four* differential equations of the first order.

lead to closed contours. This feature is similar to that in Sinai billiards and is typical for Hamiltonian systems. As the energy is increased, larger and larger parts of the Poincaré plane correspond to the chaotic motion, signifying deeper and deeper chaos – see the bottom panel of Fig. 9.

9.4. Chaos and turbulence

This extremely short section consists of essentially just one statement, extending the discussion in Sec. 8.5. The (re-) discovery of the deterministic chaos in systems with just a few degrees of freedom in the 1960s has changed the tone of the debates concerning turbulence origins, very considerably. At first, an extreme point of view that equated the notions of chaos and turbulence, became the debate's favorite.[23] However, after the initial excitement, a significant role of the Richardson-style energy-cascade mechanisms, involving many degrees of freedom, were rediscovered and could not be ignored any longer. To the best knowledge of this author, who is a distant albeit interested observer of that field, most experimental and numerical-simulation data carry features of both mechanisms, so the debate continues.[24] Due to the age difference, most readers of these notes have much better chances than the author to see where this discussion eventually leads.[25]

9.5. Exercise problems

9.1. Generalize the reasoning of Sec. 1 to an arbitrary 1D map $q_{n+1} = f(q_n)$, with the function $f(q)$ differentiable at all points of interest. In particular, derive the condition of stability of an N-point limit cycle $q^{(1)} \to q^{(2)} \to \ldots \to q^{(N)} \to q^{(1)} \ldots$

9.2. Use the stability condition derived in the previous problem, to analyze the possibility of deterministic chaos in the so-called *tent map*, with

$$f(q) = \begin{cases} rq, & \text{for } 0 \le q \le ½, \\ r(1-q), & \text{for } ½ \le q \le 1, \end{cases} \qquad \text{with } 0 \le r \le 2.$$

9.3. Find the conditions of existence and stability of fixed points of the so-called *standard circle map*:

$$q_{n+1} = q_n + \Omega - \frac{K}{2\pi} \sin 2\pi q_n,$$

where q_n are real numbers defined modulo 1 (i.e. with $q_n + 1$ identified with q_n), while Ω and K are constant parameters. Discuss the relevance of the result for phase locking of self-oscillators – see, e.g., Sec. 5.4.

[23] An important milestone in that way was the work by S. Newhouse *et al., Comm. Math. Phys*. **64**, 35 (1978), who proved the existence of a strange attractor in a rather abstract model of fluid flow.

[24] See, e.g., U. Frisch, *Turbulence*: *The Legacy of A. N. Kolmogorov*, Cambridge U. Press, 1996.

[25] The reader interested in deterministic chaos as such may like to have a look at a very popular book by S. Strogatz, *Nonlinear Dynamics and Chaos*, Westview, 2001.

9.4. Find the conditions of existence and stability of fixed points of the so-called *Hénon map*:[26]

$$q_{n+1} = 1 - aq_n^2 + p_n,$$
$$p_{n+1} = bq_n, \quad \text{with } 0 < b < 1.$$

9.5. Is the deterministic chaos possible in our "testbed" problem shown in Fig. 2.1? What if an additional periodic external force is applied to the bead? Explain your answers.

[26] This map, first explored by M. Hénon in 1976 (for a particular set of constants a and b), has played an important historic role in the study of strange attractors.